Geochemistry Geophysics Geosystems G³
AN ELECTRONIC JOURNAL OF THE EARTH SCIENCES
Published by AGU and the Geochemical Society

Article
Volume 4, Number 12
13 December 2003
8515, doi:10.1029/2003GC000609
ISSN: 1525-2027

Morphology and segmentation of the western Galápagos Spreading Center, 90.5°–98°W: Plume-ridge interaction at an intermediate spreading ridge

John Sinton
Department of Geology and Geophysics, University of Hawai'i, Honolulu, Hawai'i 96822, USA (sinton@hawaii.edu)

Robert Detrick and J. Pablo Canales
Department of Geology and Geophysics, Woods Hole Oceanographic Institution, Woods Hole, Massachusetts 02543, USA (rdetrick@whoi.edu)

Garrett Ito
Department of Geology and Geophysics, University of Hawai'i, Honolulu, Hawai'i 96822, USA (gito@hawaii.edu)

Mark Behn
Department of Terrestrial Magnetism, Cargegie Institution of Washington, 5241 Broad Branch Road, Washington, DC, 20015, USA (behn@dtm.ciw.edu)

[1] Complete multibeam bathymetric coverage of the western Galápagos Spreading Center (GSC) between 90.5°W and 98°W reveals the fine-scale morphology, segmentation and influence of the Galápagos hot spot on this intermediate spreading ridge. The western GSC comprises three morphologically defined provinces: A Western Province, located farthest from the Galápagos hot spot west of 95°30′W, is characterized by an axial deep, rift valley morphology with individual, overlapping, E-W striking segments separated by non-transform offsets; A Middle Province, between the propagating rift tips at 93°15′W and 95°30′W, with transitional axial morphology strikes ∼276°; An Eastern Province, closest to the Galápagos hot spot between the ∼90°50′W Galápagos Transform and 93°15′W, with an axial high morphology generally less than 1800 m deep, strikes ∼280°. At a finer scale, the axial region consists of 32 individual segments defined on the basis of smaller, mainly <2 km, offsets. These offsets mainly step left in the Western and Middle Provinces, and right in the Eastern Province. Glass compositions indicate that the GSC is segmented magmatically into 8 broad regions, with Mg # generally decreasing to the west within each region. Striking differences in bathymetric and lava fractionation patterns between the propagating rifts with tips at 93°15′W and 95°30′W reflect lower overall magma supply and larger offset distance at the latter. The structure of the Eastern Province is complicated by the intersection of a series of volcanic lineaments that appear to radiate away from a point located on the northern edge of the Galápagos platform, close to the southern limit of the Galápagos Fracture Zone. Where these lineaments intersect the GSC, the ridge axis is displaced to the south through a series of overlapping spreading centers (OSCs); abandoned OSC limbs lie even farther south. We propose that southward displacement of the axis is promoted during intermittent times of increased plume activity, when lithospheric zones of weakness become volcanically active. Following cessation of the increased plume activity, the axis straightens by decapitating southernmost OSC limbs during short-lived propagation events. This process contributes to the number of right stepping offsets in the Eastern Province.

Components: 11,562 words, 12 figures, 2 tables.

Keywords: Mid-ocean ridges; mantle plumes; segmentation.

Index Terms: 3035 Marine Geology and Geophysics: Midocean ridge processes; 3045 Marine Geology and Geophysics: Seafloor morphology and bottom photography; 8121 Tectonophysics: Dynamics, convection currents and mantle plumes.

Received 26 July 2003; **Revised** 16 October 2003; **Accepted** 17 October 2003; **Published** 13 December 2003.

Sinton, J., R. Detrick, J. P. Canales, G. Ito, and M. Behn, Morphology and segmentation of the western Galápagos Spreading Center, 90.5°–98°W: Plume-ridge interaction at an intermediate spreading ridge, *Geochem. Geophys. Geosyst.*, *4*(12), 8515, doi:10.1029/2003GC000609, 2003.

Theme: Plume-Ridge Interaction

1. Introduction

[2] The morphology of mid-ocean ridges tends to vary with spreading rate [*Macdonald*, 1982]. Those ridges with full spreading rates <50 mm/yr typically have axial valleys, 1–2 km deep and 15–30 km wide, whereas ridges spreading at >80 mm/yr are commonly associated with a 2–10 km wide, 200–400 m axial high, flanked by smoother abyssal topography. It has long been known that mid-ocean ridges spreading at intermediate rates can show a range of axial morphology, varying from axial valleys similar to those of slow-spreading ridges to axial highs similar to those of faster spreading ridges. The Galápagos Spreading Center (GSC) is an intermediate spreading rate mid-ocean ridge (Figure 1), with full spreading rates varying from 45 mm/yr at 98°W to 63 mm/yr at 86°W [*DeMets et al.*, 1994]. The spreading rate is 57 mm/yr near the Galápagos Transform at 90°50′W. *Schilling et al.* [1982] and *Canales et al.* [1997] documented systematic variation in axial morphology along the GSC, which they related to the influence of the Galápagos hot spot, centered in the region 91°–92° W. Prior to the G-PRIME expedition [*Sinton et al.*, 2000; *Detrick et al.*, 2002] multibeam bathymetric mapping was incomplete along the western Galápagos spreading center. *Hey et al.* [1986] produced the first multibeam map of the local region around the 95°30′W propagating/failing rift system. *Canales et al.* [1997] reported the results of a much more extensive, although still incomplete, survey of the spreading center encompassing the eastern GSC from 85°W–90°W, and the western GSC between 93°30′W and 95°W. Owing to technical difficulties, no swath bathymetry data were collected for the shallowest region between 90°W and 93°30′W in that study. In addition, *Searle* [1989] identified and described the large-scale segmentation of the GSC west of 95°W.

[3] In this paper we present the results of continuous multibeam bathymetric mapping of the axial region of the GSC between the Galápagos transform near 90°50′W and 98°W. These new bathymetric data allow us to identify the fine-scale segmentation of the spreading center, as well as document the details in axial morphology and its variation along axis. In particular, the axial region closest to the assumed location of the center of the Galápagos hot spot between 91°W and 92°W has been mapped at high resolution for the first time. The fine-scale structure of this region reflects interaction between the spreading center and the nearby mantle plume.

2. Tectonic Setting

[4] The east-west striking GSC separates the Cocos and Nazca plates in the eastern equatorial Pacific (Figure 1). At 91°W, the GSC lies ∼200 km north of the Galápagos Archipelago, the western end of which marks the probable center of the Galápagos mantle plume [*White et al.*, 1993]. Although the Galápagos plume may have been active for more than 90 Ma [*Sinton et al.*, 1998], the GSC formed only about 23–25 Ma [*Hey*, 1977; *Barckhausen et al.*, 2001; *Meschede and Barckhausen*, 2001]. The GSC has been strongly influenced by the hot spot

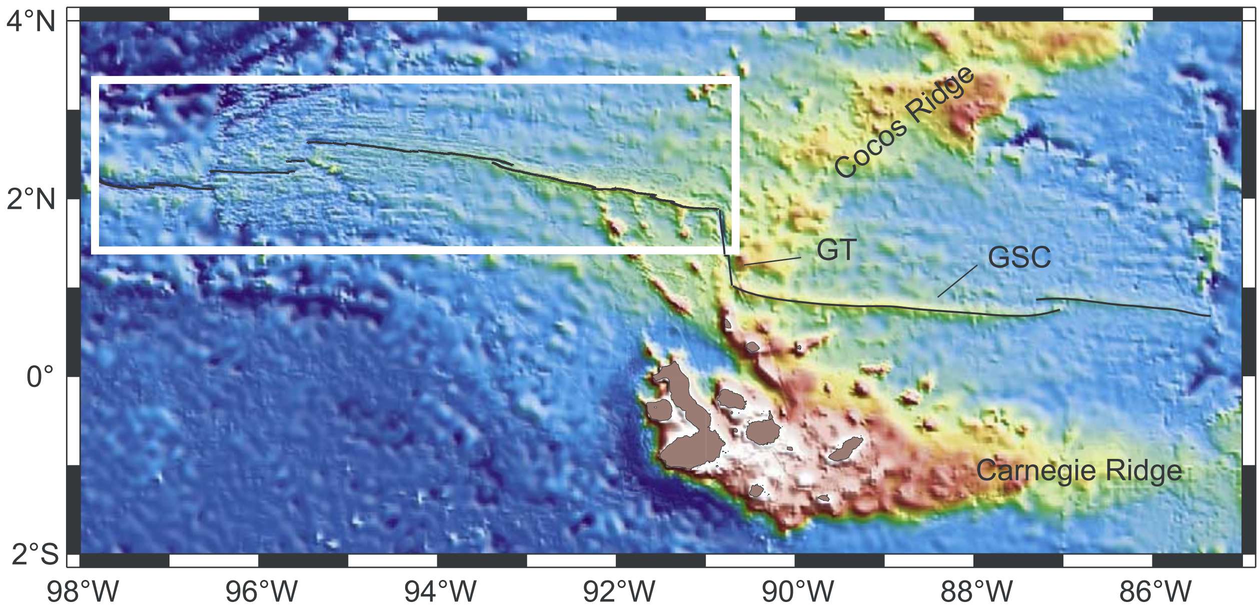

Figure 1. Map of the Galápagos area based on integration of available multibeam bathymetry (Figure 2) and satellite-derived seafloor topography data [*Smith and Sandwell*, 1997]. Water depths range from >3500 m (blue) to <1000 m (red). The axis of the east-west trending Galápagos Spreading Center (GSC) is shown by a black line. The ~100-km-long Galápagos Transform (GT) near 90.5°W connects the western GSC to the eastern GSC. The presumed center of the Galápagos hot spot is in the western part of the Galápagos Archipelago (islands shown in brown). White box encloses the area of Figure 2.

throughout its history [*Vogt*, 1976; *Hey*, 1977; *Morgan*, 1978]. For much of this history the ridge has been nearly centered over the Galápagos hot spot, producing the Cocos and Carnegie aseismic ridges that track the absolute motion of the Cocos and Nazca plates in the hot spot reference frame [*Hey*, 1977]. The tectonic history of the GSC has been dominated by asymmetric accretion and rift propagation [*Hey*, 1977; *Wilson and Hey*, 1995; *Barckhausen et al.*, 2001]. As the GSC migrated northward away from the hot spot, ridge jumps predominantly to the south have kept the axis of the spreading center close to the hot spot. Propagating rift tips are located within the study area at 95°30′W and 93°15′W (Figure 2). According to the magnetic data and reconstruction of *Wilson and Hey* [1995], the present Galápagos Transform apparently formed 2.6–3.6 Ma; since that time the GSC has been progressively migrating to the north, away from the hot spot.

3. Segmentation of the Western GSC

[5] The western GSC is separated from the eastern GSC by the ~100-km long Galápagos Transform near 90°50′W (Figure 1). The western GSC is segmented at the coarsest scale by the large offsets coinciding with the propagating rift tips near 93°15′W and 95°30′W, and large, over-lapping, non-transform offsets near 95°40′W and 96°30′W (Figure 2, Table 1). The two major propagating rifts separate three large provinces of the axial region defined by differences in axial morphology and the trend of the axis, which becomes more E-W with increasing distance west of the Galápagos transform. The trend of the ridge axis is approximately 280° between the Galápagos Transform and the propagating, overlapping spreading center (OSC) near 93°15′W (Figure 2), 276° between the propagating rift tips at 93°15′W and 95°30′W, and nearly east-west (~272°) west of 95°30′W to the limit of our study area near 98°W. We refer to these large regions as the Eastern, Middle and Western Provinces of the western GSC.

[6] It is notable that there apparently are no simple transform faults in the area. The Galápagos Transform strikes ~355° and therefore the transform-GSC intersection is about 15° oblique. If the spreading direction is nearly normal to the ridge,

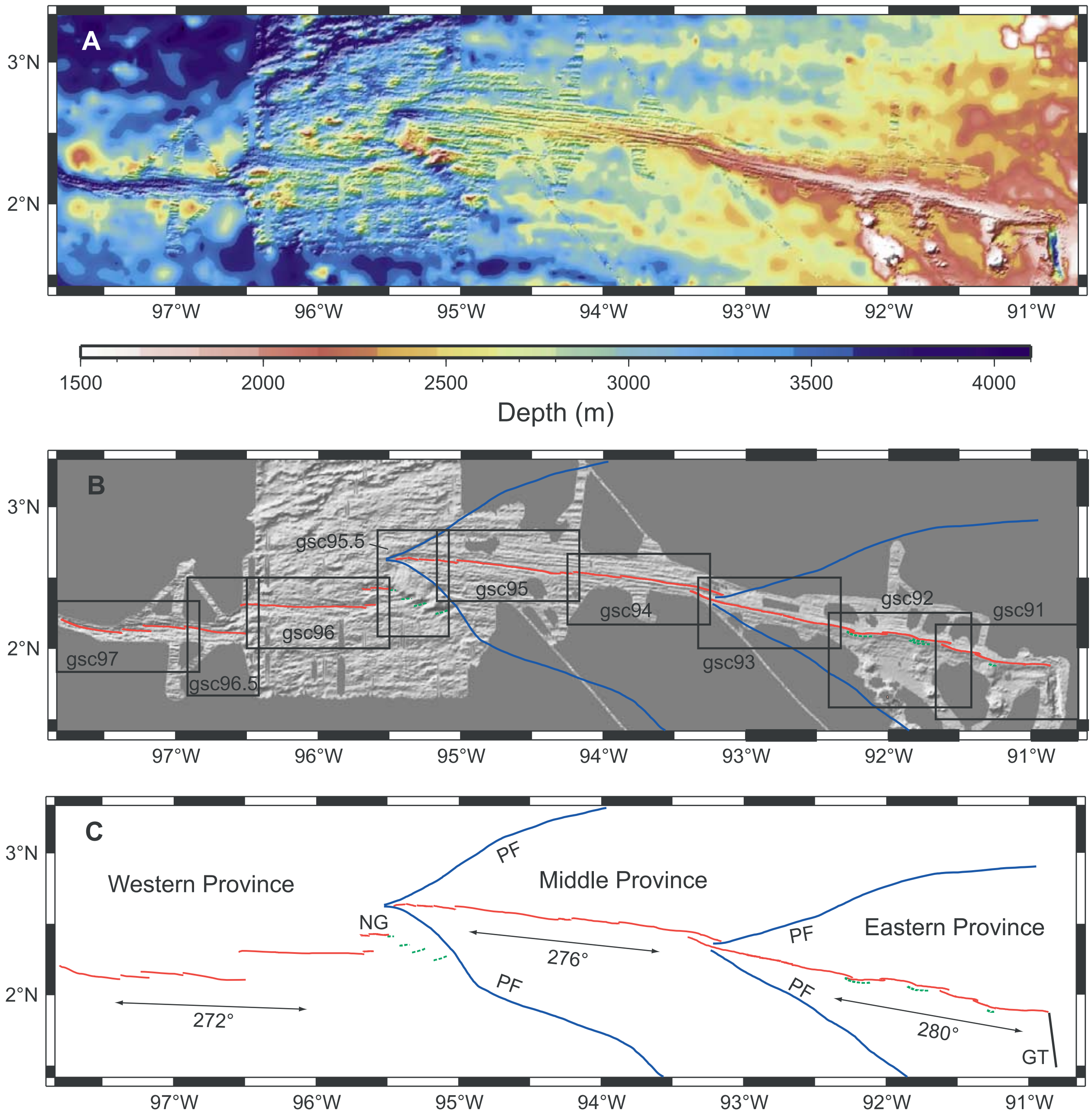

Figure 2. (a) Bathymetric map of the western GSC between 90.5 and 98°W; bathymetry based on multibeam data available from National Geophysical Data Center, new data collected during this study, *Canales et al.* [1997], the AHA-NEMO2 expedition (D. Fornari, M. Perfit, M. Tolstoy, R. Haymon, D. Scheirer, P. Johnson, G. Kurras, S. White, J. Getsiv, and shipboard scientific and technical party, AHA-NEMO2, shipboard data web site compiled during R/V Melville NEMO Expedition, Leg 2, available at http://science.whoi.edu/ahanemo2/, 2000) and Sonne Cruise 158 (R. Werner, personal communication, 2002), merged with satellite-derived seafloor topography data [*Smith and Sandwell*, 1997]. (b) Shaded relief image showing multibeam coverage for this area. Boxes outline areas of individual GMT grids and maps (postscript format) available as downloads from http://www.soest.hawaii.edu/GG/FACULTY/SINTON/GSC.html. In B and C the rift axis is shown by a red line. Pseudofaults (PF) of propagating rifts with tips at 95°30′W and 93°15′W are shown by blue lines after *Wilson and Hey* [1995]; abandoned or failed rifts are shown as green dotted lines. (c) Division of the western GSC into provinces defined by major offsets, changes in average ridge axis orientation, and morphology. NG, North Graben; GT, Galápagos Transform.

Table 1. Western Galápagos Spreading Center Segments[a]

Segment	Longitude, W Start	Longitude, W End	Seg. Length, km	Offset, km	Offset type
				100	**Galápagos Transform**
Eastern Province					
E1	90.862	91.233	52.0	0.4	LS
E2	91.233	91.389	19.6	1.4	RS OSC
E3	91.356	91.619	32.6	3.5	RS OSC
E4	91.558	91.787	26.5	0	DevAL
E5	91.790	92.043	30.2	1.6	LS OSC
E6	92.009	92.266	30.5	1.9	RS OSC
E7	92.238	92.508	32.4	0	DevAL
E8	92.508	92.662	17.9	0.5	RS
E9	92.657	92.739	9.7	0.5	RS
E10	92.741	92.888	17.1	0.5	RS
E11	92.888	92.975	10.2	0.3	RS
E12	92.978	93.393	49.4		
				6.8	**RS PR/OSC**
Middle Province					
M1	93.158	93.878	84.9	1.0	LS
M2	93.875	94.208	40.5	0.9	LS
M3	94.214	94.300	10.6	0.6	LS
M4	94.301	94.394	10.2	0.5	RS
M5	94.395	95.029	70.5	1.9	LS
M6	95.024	95.180	20.2	0.6	LS
M7	95.108	95.293	12.6	0.5	LS
M8	95.299	95.369	7.4	0.5	LS
M9	95.374	95.456	10.6		
				22.2	**LS PR**
Western Province					
NG-1	95.482	95.629	15.7	1.3	LS
NG-2	95.631	95.682	5.7		
				12.0	**LS NTO**
W1-1	95.597	95.669	8.3	1.8	LS
W1-2	95.663	95.898	27.4	0	DevAL
W1-3	95.898	96.063	18.3	0	DevAL
W1-4	96.023	96.413	39.0	0	DevAL
W1-5	96.430	96.545	15.2		
				22.9	**LS NTO**
W2-1	96.465	96.937	51.8	1.8	LS
W2-2	96.933	97.232	33.9	4.1	LS
W2-3	97.171	97.373	22.6	3.0	LS
W2-4	97.376	97.801	>50.0	?	?

[a] E, Segments of the Eastern Province; M, segments in the Middle Province W, NG, Segments in the Western Province, including North Graben. LS, left stepping; RS, right stepping; OSC, overlapping spreading center; DevAL, deviation in axial linearity; PR, propagating rift tip; NTO, non-transform offset.

e.g., as argued by *Harpp and Geist* [2002], consistent with the rotation pole of *Wilson and Hey* [1995], then the transform must be in extension. Alternatively, if the GSC spreading direction is parallel to the transform strike (oblique spreading, similar to the Reykjanes Ridge in the north Atlantic), then the transform need not be in extension. Our mapping shows the presence of several intratransform volcanoes (Figure 3), indicating at least some extension within the transform zone. Our results do not, however, provide additional constraints on the precise spreading direction in this region. Other offsets in the area are either propagating rifts or overlapping, non-transform offsets.

[7] We have further subdivided the Eastern, Middle and Western Provinces by noting all discontinuities in the axis with offsets $\geq$0.3 km and sudden bends or kinks in the strike of the ridge axis of >5° (deviations in axial linearity or DevALs [*Langmuir*

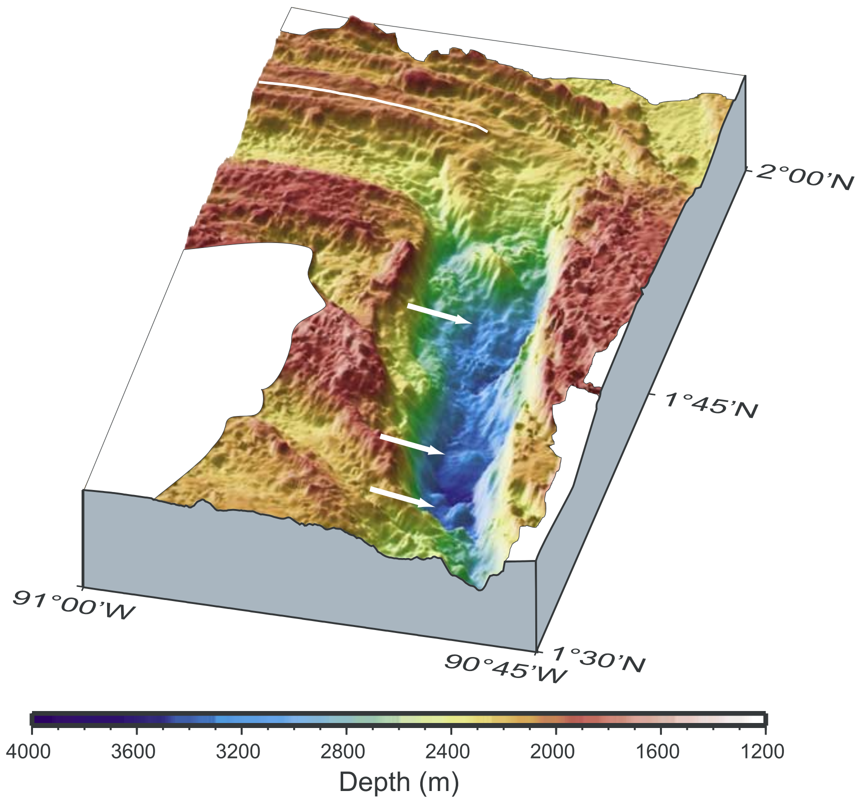

Figure 3. Shaded relief, oblique view of the Galápagos transform zone. GSC axis is shown as white line. At least three volcanic cones present within the deep part of the transform zone south of 1°50'N are indicated by arrows. Dredging during G-PRIME confirms that these are volcanoes.

et al., 1986] (Table 1). Where the axis shows a smooth curve over greater distances, we consider it to be a part of a single segment. The offsets separating these smaller-scale segments are mainly less than 2.0 km, with two larger offsets in the Western Province. In the Eastern Province ten of the 12 identified segments are separated by right-stepping offsets. In contrast, segment offsets in the Middle and Western Provinces are almost exclusively left stepping, with only one right-stepping offset identified in the Middle Province (Table 1, Figure 2c). Left-stepping offsets continue to dominate the GSC to its limit near 101.8°W [*Searle*, 1989], with one right-stepping offset at the boundary of our study area near 98°W. The one major offset in the eastern GSC near 87°W also is left stepping (Figure 1), although the Galápagos Transform steps right. Thus with the exception of the Eastern Province, the GSC is dominated by left-stepping offsets over most of its length from the Inca Transform near 85.5°W to its intersection with the Galápagos microplate near 102°W. It is well known that individual spreading centers have a preference for step direction over considerable lengths [e.g., *Lonsdale*, 1985], which can be a response to changes in spreading direction [*Nelson*, 1981]. The predominance of left stepping offsets along the GSC is consistent with a clockwise rotation of the spreading direction. *Wilson and Hey* [1995] documented clockwise rotations of the GSC at ~7 Ma, and again at 1.5 Ma. We interpret the anomalous, right-stepping offsets in the Eastern Province of the western GSC to reflect a southward migration of the easternmost axis in response to interaction of the ridge with the Galápagos hot spot.

[8] From west to east, the strike of the western GSC axis becomes progressively more SE. *Wilson and Hey* [1995] and *Meschede and Barckhausen* [2001] documented a history of mainly south-stepping ridge jumps as the GSC has attempted to minimize the ridge-hot spot separation. As the

hot spot is approached from the west, the GSC continuously steps to the south, which reduces the ridge-hot spot distance. This results in a series of right-stepping offsets and a diversion of the regional ridge strike to a more southeasterly orientation. In addition, the detailed tectonic history of the near-hot spot region (see Section 7.2) also contributes to the development of right-stepping offsets in the Eastern Province.

4. Axial Depth and Morphology

[9] The western GSC shows large variations in axial depth and morphology (Figures 4, 5, 6, 7, and 8) [*Schilling et al.*, 1976, 1982; *Christie and Sinton*, 1981; *Phipps Morgan and Parmentier*, 1985; *Canales et al.*, 1997]. Most of the Eastern Province is dominated by a topographic high that rises to 600 m above seafloor depths 5 km off axis (Figure 4). The axial high in the Eastern Province tends to be higher and wider than axial highs along the East Pacific Rise [e.g., *Scheirer and Macdonald*, 1993], although considerable variation exists for fast spreading ridges [*Macdonald and Fox*, 1988]. *Carbotte and Macdonald* [1994] attributed wider and higher axial highs at intermediate spreading ridges, compared to fast spreading ridges, to a stronger lithosphere that is better able to support volcanic loading. The anomalously high magma supply associated with the Galápagos hot spot in the Eastern Province presumably contributes to the dimensions of the axial high in this region. Axial depth and roughness both increase westward within the Middle Province (Figure 8a), which is characterized by a transitional morphology displaying neither an axial valley nor a topographic high (Figure 5). The Western Province is characterized by axial depths mainly >3000 m, with the axis lying in valleys approximately 10 km wide and up to 800 m deep (Figure 6). The axial depth profile (Figure 8a) in the Western Province is very rough. The high local relief of this area is mainly a consequence of the large number of small seamounts in the axial region [*Detrick et al.*, 2002; *Behn et al.*, 2003].

[10] Thus there are strong correlations among axial morphology, axial depth and bathymetric roughness for the three provinces defined on differences in axial strike and the presence of major offsets. However, within each province there are gradations in depth, morphology and roughness. For example, although the morphology of the Eastern Province is generally characterized by a broad axial high, the high can locally be cut by a narrow trough (Figure 4). Between 91°40′W and 91°47′W (western part of segment E4), the axis lies in a trough ~0.5 km wide and 50 m deep; near 92.38°W the axis lies in a fault-bounded trough or graben that is about 2 km wide, although only about 40 m deep. Farther to the west this graben persists and gradually deepens. It is the first appearance of this persistent, axial trough that *Detrick et al.* [2002] emphasized as correlating with a rapid change in the depth to the axial magma chamber seismic reflector and the boundary between mildly incompatible-element-enriched T-MORB to the west and more strongly enriched E-MORB to the east.

[11] The transitional morphology of the Middle Province is generally characterized by a horst and graben structure, which comprises the near-axis abyssal hill fabric. The axis lies exclusively within axial graben (Figure 5). In contrast to the Eastern Province, the axis of the Middle Province is not elevated relative to the near-axis structure (Figure 7). The Middle Province can be sub-divided into three regions, each with distinct morphology and gradient in axial depth. East of 93°50′W the alternating horsts and graben average about 2 km in width, but this wavelength generally increases to the west. From 93°50′W to ~94°23′W (segments M2–M4) the axial region consists of alternating horsts and graben averaging about 3–3.5 km in width (Figure 5b); the location of the current spreading axis is difficult to define precisely in this region. The axis gradually deepens westward between the 93°15′W offset and 94°23′W at about 2–2.5 m/km. West of 94°23′W the axis of segment M5 lies in a well-defined graben that widens and deepens westward at about 4 m/km. By the western end of segment M6 near 95°11′W the axis lies in a graben ~5 km wide and more than 250 m deep. West of 95°11′W the axis deepens rapidly (Figures 5c and 8a) at about 9.5 m/km, and the axial graben widens to ~9 km. Between 95°19′W and 95°30′W,

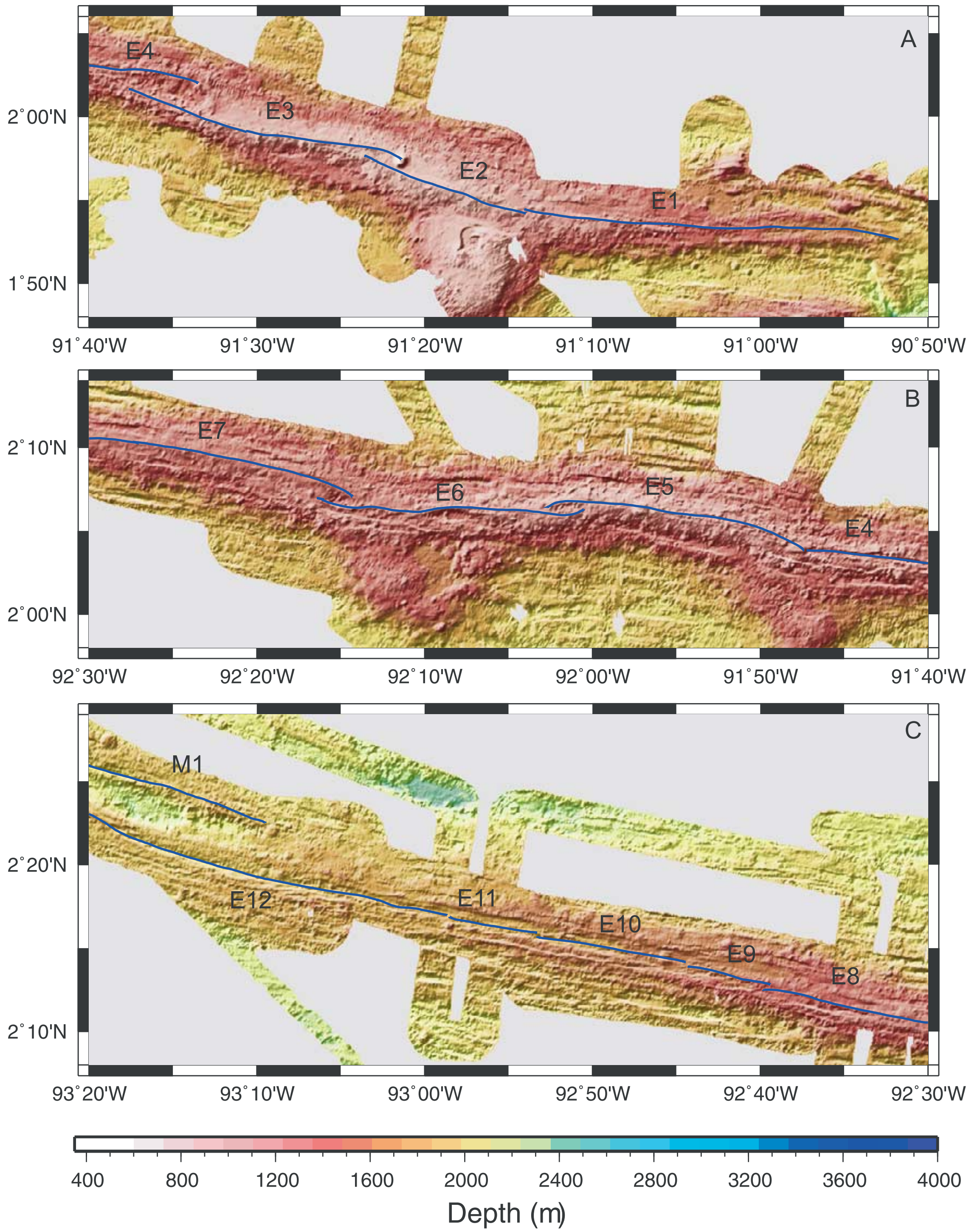

Figure 4. Shaded relief images of multibeam bathymetry of the Eastern Province of the western GSC; illumination direction is from the NW. Individual segments (Table 1) are labeled. All segments of the Eastern Province have an axial high morphology. Our interpretation of the current spreading axis is shown by the blue lines.

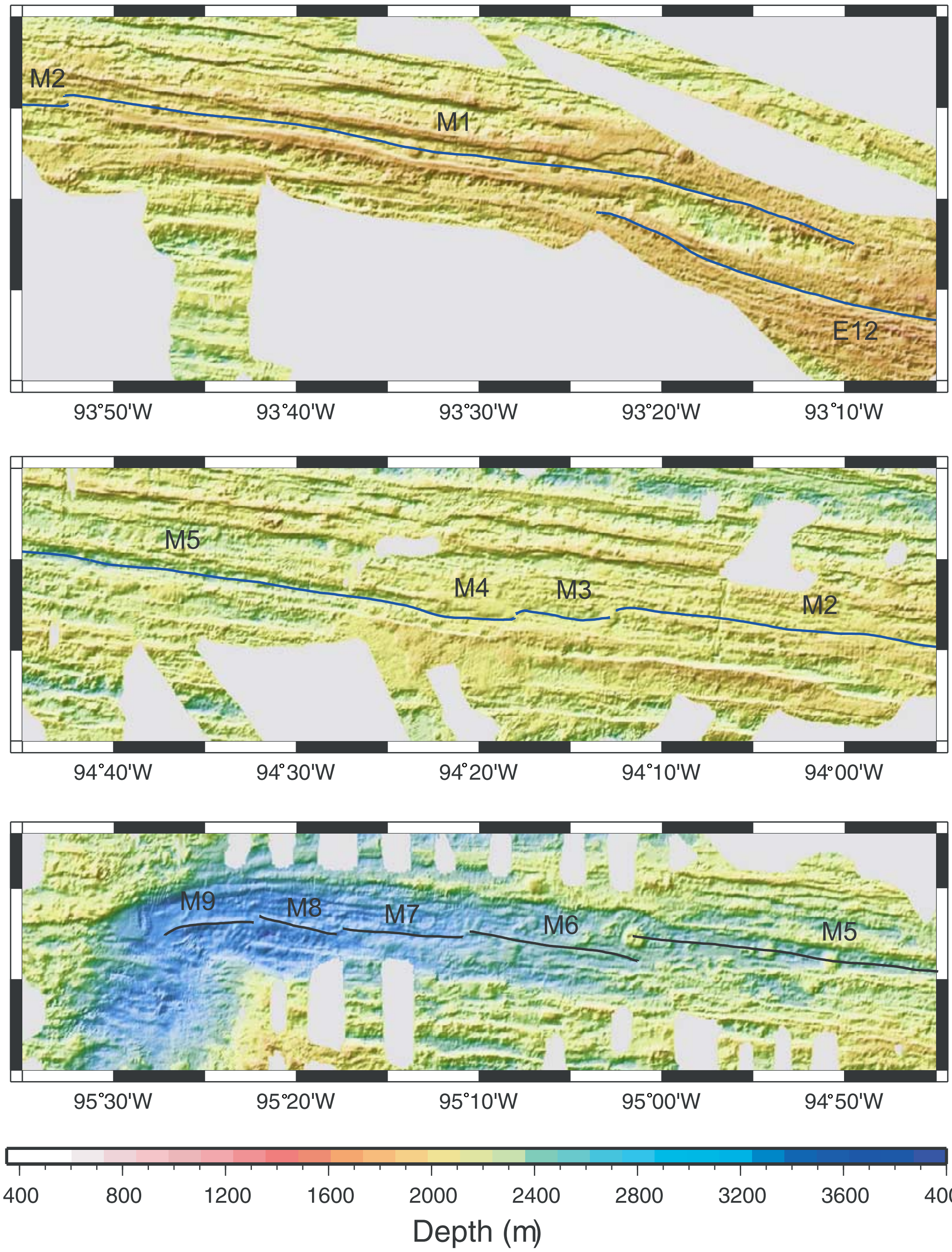

Figure 5. Shaded relief images of multibeam bathymetry of the Middle Province of the western GSC; illumination direction is from the NW. Individual segments (Table 1) are labeled; our interpretation of the current spreading axis is indicated.

the axis is a narrow ridge within a wider graben. The axial ridge of segment M9 gradually bends to the south as the propagating rift tip is approached and intersects the inner pseudofault near 95°30s [*Hey et al.*, 1989; *Kleinrock and Hey*, 1989]. The rapid deepening of the axis west of 95°11′W suggests that this is the region most strongly affected by the propagating rift that terminates near 95°30′W [*Hey*, 1977; *Hey et al.*, 1989].

[12] Within the Western Province the axis is difficult to define precisely. The overall structure is a

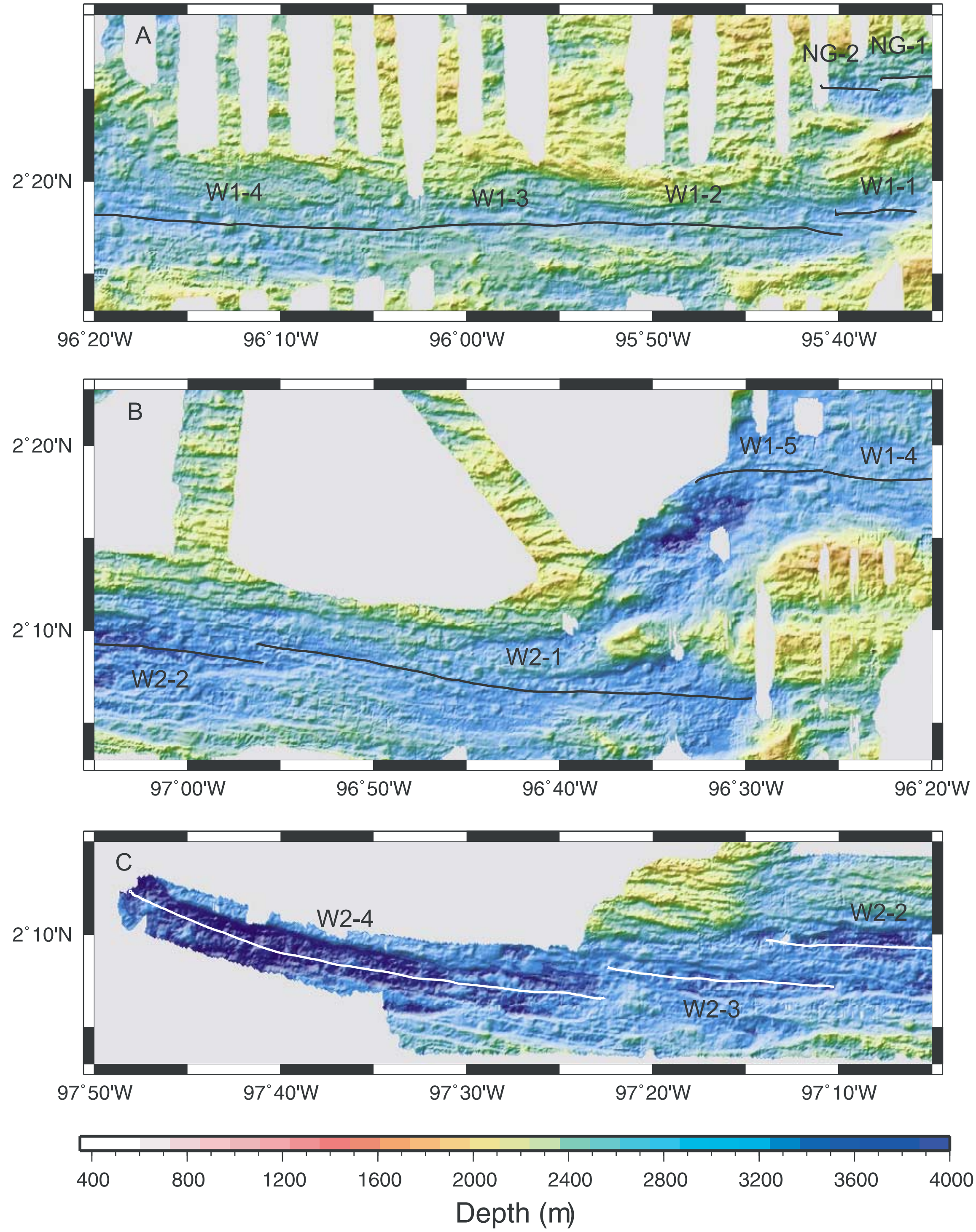

Figure 6. Shaded relief images of multibeam bathymetry of the Middle Province of the western GSC; illumination direction is from the NW. Individual segments (Table 1) are labeled; our interpretation of the current spreading axis is indicated.

10.1029/2003GC000609

Figure 7. Cross-axis topographic profiles showing range of axial morphologies. Those east of 92.7°W (red) have axial high morphology, those between 92.7°W and 95.5°W (green) have transitional morphology and those west of 95.5°W (blue) have axial valley morphology. Segment designation (left - Table 1) and longitudes (right) are shown for each profile.

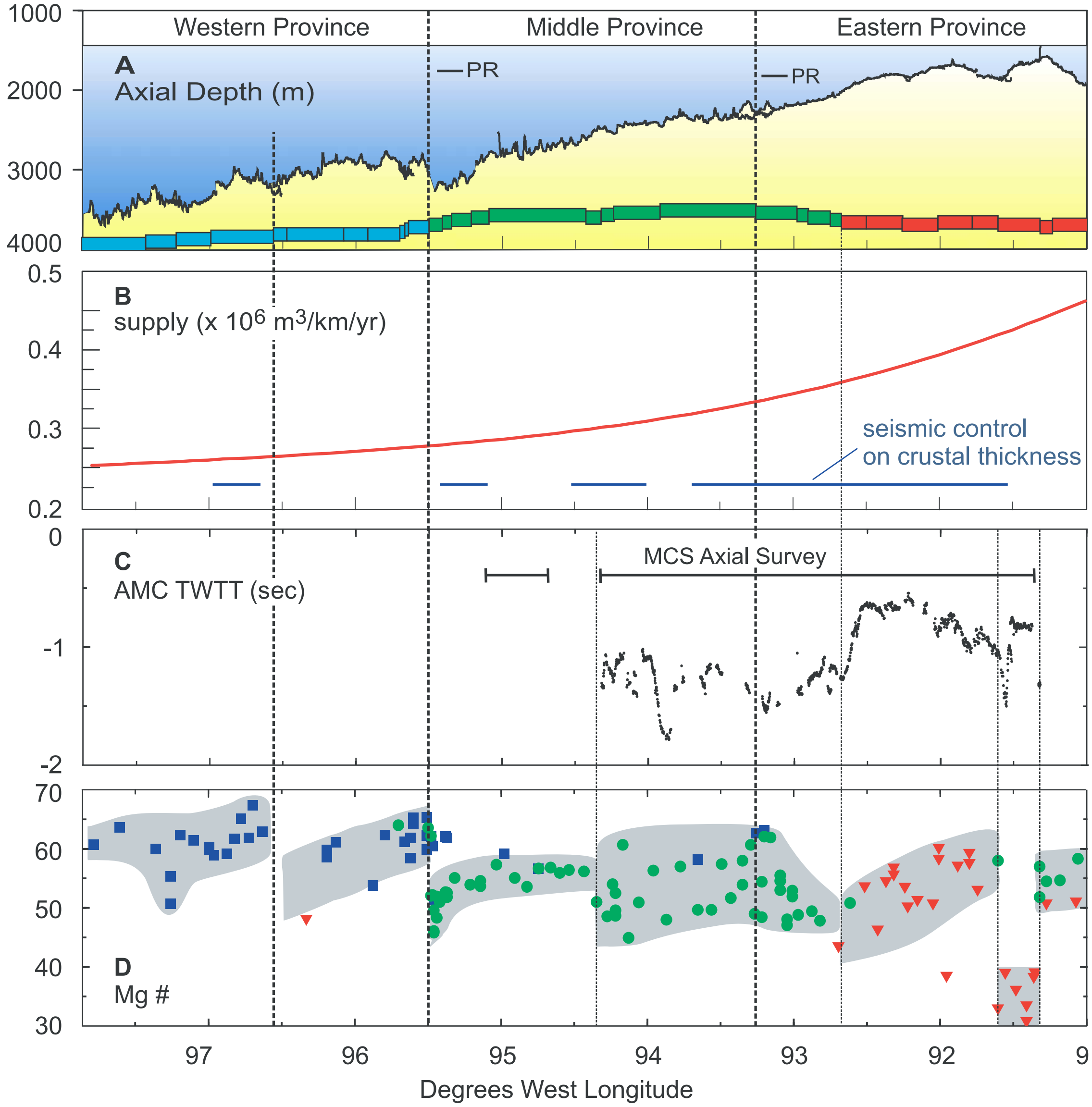

Figure 8. Along-axis profiles. Major tectonic boundaries are shown by heavy dashed lines. Light dashed lines indicate other boundaries discussed in the text. (a) Bathymetry, segmentation and axial morphology. Axial depth profile shows water depth along the present spreading axis. Top panel shows coarse segmentation into three provinces from Figure 2. Smaller-scale segmentation (Table 1) and axial morphology are shown by the colored rectangles where red, axial high; green, transitional, and blue, axial deep. Sense of offset (not to scale) between the smaller segments is indicated; DevAls shown without offset. (b) Crustal production rate calculated as crustal thickness [from *Detrick et al.*, 2002] x spreading rate (Nuvel 1A [*DeMets et al.*, 1994]). Regions where we have seismic constraints on crustal thickness [from *Detrick et al.*, 2002; *Canales et al.*, 2002] are shown by horizontal lines. (c) Axial magma chamber (AMC) seismic reflector detected by MCS survey along axis [*Blacic et al.*, 2002; *Detrick et al.*, 2002]; survey was run off axis between 94°42′W and 94°21′W. (d) Variation in glass Mg # [from *Detrick et al.*, 2002]; regions of smoothly varying Mg # are shaded. Samples are keyed to chemical affinity based on K/Ti [*Detrick et al.*, 2002], as follows: N-MORB (blue squares); T-MORB (green circles) and E-MORB (inverted red triangles). See text for discussion.

series of axial rift valleys that vary from about 8 to 14 km in width (Figure 6). Within the axial valleys are numerous small seamounts [*Behn et al.*, 2003]. For the most part, these seamounts show a nearly random distribution and do not appear to be aligned into chains. The axial structure and segmentation are mainly defined by broad overlapping rift graben. The off-axis topographic discontinuity at 97°15′W (Figure 6) extends to the limit of our data coverage, indicating that the overlapping boundary between segments W2-2 and W2-3 has persisted for at least 350 ka.

5. Axial Magma Chambers and Magmatic Segmentation

[13] The regional variations in morphology and axial depth can be related to variations in magma supply along the GSC. Because we have measured the variation in crustal thickness throughout the region [*Canales et al.*, 2002; *Detrick et al.*, 2002], we are able to calculate the crustal production rate along axis, incorporating changes in crustal thickness and spreading rate (Figure 8b). To a first order, crustal production rate corresponds to the rate of magma supply to the axis, which we describe as a volume flux per unit length of ridge axis. Thus the change from axial high to transitional morphology coincides with a supply rate of 0.357×10^6 m^3/km/yr (1 km length of spreading center axis). West of the PR tip at 95°30′W, where the axis lies in broad axial valleys, the supply is less than 0.277×10^6 m^3/km/yr. Using multichannel seismic (MCS) profiling [*Blacic et al.*, 2002; *Detrick et al.*, 2002], we were able to detect a strong reflector corresponding to an axial magma chamber (AMC) as far west as 94°22′W. Although we continued MCS profiling to 95°12′W, with a gap in axial coverage between 94°22′W and 94°42′W, no AMC reflectors were detected in the axial survey area west of 94°42′W; thus the disappearance of the seismically detectable AMC coincides with a supply rate of $\sim 0.30 \times 10^6$ m^3/km/yr (Figures 8b and 8c).

[14] Variations in lava geochemistry can be used to decipher aspects of magmatic segmentation along axis. *Detrick et al.* [2002] showed that the three broad regions of axial morphology generally correspond to variation in incompatible element ratios that are interpreted to reflect the composition of parental magmas supplying the axis. East of 92°40′W the axis is dominated by the eruption of incompatible-element-enriched (E-) MORB; the region between 92°40′W and the PR tip at 95°30′W is dominated by the eruption of transitional (T-) MORB, while normal (N-) MORB dominate the axis farther to the west [*Cushman et al.*, 2001].

[15] Another aspect of magmatic segmentation is reflected in glass Mg # (molar MgO/(MgO + FeO*)), where FeO* is total Fe as FeO. Eight regions, each characterized by smoothly varying Mg #, are delineated in Figure 8d. Because Mg # generally correlates with magmatic temperature, the boundaries separating these regions presumably reflect discontinuities in thermal structure of the axial crust, which can be affected by overall magma supply, the size, longevity and recharge of axial magma chambers, and the extent of hydrothermal cooling along axis. Most of these boundaries coincide with major tectonic boundaries discussed previously, as shown by heavy dashed lines in Figure 8, including the 96°30′W NTO, and the major propagating rifts. In contrast, the 92°40′W boundary is not a major tectonic offset, although it marks the first appearance of persistent axial troughs and the boundary between regions dominated by E-MORB and T-MORB. It is notable that segment E3 (Figure 4a) in the highly inflated region near 91°30′W contrasts with segments on either side in being dominated by highly evolved (low Mg #) E-MORB in a region of highly variable AMC depth. This result is unexpected and suggests that this segment has either not received recent recharge of magma from the mantle or else it is experiencing unusual amounts of cooling, presumably from vigorous hydrothermal activity.

[16] The variability in Mg # shows an interesting saw-tooth pattern along the ridge axis (Figure 8d). Mg # tends to decrease to the west within each magmatic segment, then step to higher Mg # across each segment boundary. This pattern is most pronounced for the segment between 91°30′W and 92°40′W, and the two magmatic segments of the Western Province. Such a pattern might be

expected if these broad magmatic segments are propagating to the west, in which case low Mg #s might be expected behind the propagating rift tips. Unfortunately, with the exception of the region around 95°30′W, off-axis bathymetric coverage is not sufficient to determine whether or not there are pseudofaults that might be associated with these putative propagating rifts. Although the most pronounced magmatic fractionation anomalies tend to be restricted to a few 10s of km behind PR tips [*Sinton et al.*, 1983], *Sinton et al.* [1991] documented a 200-km-long gradient associated with the 20.7°S propagator on the East Pacific Rise, comparable to those of Figure 8d. Alternatively, this pattern may simply reflect along-axis variations in magma supply within segments. Along the GSC gradients in magma supply associated with the hot spot might promote increased magma supply on the ends of individual segments closest to the hot spot, consistent with elevated topography on the eastern ends of these particular magmatic segments.

[17] There is an interesting change in the pattern of Mg # with longitude that occurs at 94°23′W. East of 94°23′W Mg # varies widely over short spatial scales, whereas to the west lava compositions are more uniform in a given area, with a gradient of decreasing Mg # toward the propagating rift tip. This boundary coincides with the small offset between segments M4 and M5 (Figure 5b, Table 1), and the westward transition to a distinct axial graben. It also coincides with the westward limit of the AMC reflector observed with MCS. Our MCS survey was off-axis between 94°22′W and 94°42′W, although no AMC reflector was observed for the axial survey area west of 94°42′W (Figure 8). Thus the "disappearance" of the AMC reflector is constrained only to be somewhere in the region between 94°22′W and 94°42′W. Although one might expect frequent recharge and magma mixing in shallow magma chambers to produce uniform magma compositions [*Sinton and Detrick*, 1992], our results indicate that local magma differentiation is more uniform in the region between 94°23′W and the PR tip at 95°30′W where crustal magma reservoirs were not detected by the MCS survey and thus either are not present, are present only intermittently, or are present but too small to detect. In contrast, to the east where we have a well-defined AMC, compositions are much more variable over short spatial scales. Detailed studies around the 95.5°W propagating rift [*Christie and Sinton*, 1981; *Hey et al.*, 1992] indicate that the typical lavas erupted there are relatively aphyric ferrobasalts, which *Sinton and Detrick* [1992] interpreted to have been erupted from small, melt-dominated magma reservoirs. Our results suggest that magma reservoirs smaller (<∼0.5 km wide), or more intermittent than those detectable by MCS, but with uniformly low magma supply, characterize much of the subaxial region between 94°23′W and the PR tip at 95°30′W. In contrast, east of 94°23′W magma supply is sufficiently voluminous and frequent to sustain melt lenses large enough to be detected by MCS. However, in this region the AMC reflector shows highly variable depth, corresponding with the region of highly variable Mg #, suggesting eruption from crustal reservoirs that are much more variable over smaller spatial scales with respect to local magma supply and hydrothermal cooling characteristics.

6. Propagating Rifts

[18] The evolution of the GSC has been dominated by propagating rift tectonics [*Hey*, 1977; *Schilling et al.*, 1982; *Wilson and Hey*, 1995]. Within the study area there are two major westward-propagating rifts with tips at 95°30′W and 93°15′W. Associated with the 95°30′W propagator are distinct anomalies in bathymetry and extent of lava fractionation. These two anomalies both become most pronounced within ∼35 km of the PR tip, culminating with the most fractionated lavas and deepest axis coinciding with the neovolcanic tip of the propagator [*Christie and Sinton*, 1981; *Kleinrock and Hey*, 1989; *Hey et al.*, 1989, 1992].

[19] *Kleinrock et al.* [1989] showed that the failed spreading center system associated with the 95°30′W PR is composed of a series of right-stepping, en echelon basins that extend southeastward from the failing rift of North Graben (Figures 2 and 6; segments NG-1, 2). North Graben, with an axis of symmetry near 2°25′N, is offset 12–13 km left laterally from the doomed rift. *Kleinrock et al.*

[1989] speculated that North Graben is a transient feature, which they referred to as a migrating extensional relay zone (MERZ), that formed by a northward jump in the failing axis in response to the migrating strain/stress field of the migrating transform zone of the propagator system. Although those authors considered the alternative hypothesis that North Graben represents a pre-existing offset in the doomed rift, they preferred the MERZ model because of lack of evidence for transform fault structures in the region and lack of an offset in the Brunhes-Matuyama magnetic reversal boundary off axis. However, it is now apparent that the dominant spreading center mode west of 95°30′W is overlapping axial rift graben separated by non-transform offsets. Thus our new bathymetric data in the region are consistent with North Graben representing a ∼25 km-long vestige of an axial graben that formerly was at least 60 km long; this graben has subsequently been broken into the series of en echelon failed rift graben that extend southeastward from North Graben (Figure 2b).

[20] In contrast to the correlated bathymetric and lava compositional anomalies associated with the 95°30′W PR, the 93°15′W PR has very different character. The overlapping limbs of the propagating OSC at 93°15′W are up to ∼150 m shallower than the surrounding axial ridges away from the offset (Figures 4c, 5a, and 8a), and the lavas collected from the overlapping limbs are slightly higher in Mg # than any east of 95°W. Thus the fractionation and bathymetric anomalies at the 93°15′W PR appear to be in the opposite sense of those of propagating rifts elsewhere [*Sinton et al.*, 1983]. There are a number of important differences between these two systems (Table 2) that might help explain the lack of typical fractionation and bathymetric anomalies at 93°15′W. *Christie and Sinton* [1981] and *Sinton et al.* [1983] argued that the development of magmatic fractionation anomalies at propagating rifts are a consequence of the balance between magma supply and crustal cooling of magma reservoirs. At 93°15′W, overall supply is about 20% greater than it is at 95°30′W (Table 2) and this difference might be sufficient to suppress the development of fractionation anomalies in subaxial magma reservoirs. Furthermore, the propagator at 93°15′W is breaking through crust that is only about 260 ka, compared to 910 ka at 95°30′W, and crustal cooling can therefore be expected to be much less important at 93°15′W. *Wilson and Hey* [1995] emphasized segment length and offset distance as being important in controlling fractionation anomalies as a consequence of along-axis transport of magma at crustal levels. They argued that fractionation anomalies only develop at the distal ends of segments that are more than 50 to 100-km long. Although the definition of what constitutes a segment can vary, it is clear that the strong fractionation anomaly at the 95°30′W PR is associated with several small segments, all of which either individually or combined are shorter than the relatively long segment that leads to the 93°15′W PR. As such, fractionation anomalies for these two propagating rift systems do not appear to depend on segment length in the way predicted by *Wilson and Hey* [1995]. *Wilson and Hey* [1995] also noted the importance of offset distance, although they emphasized the role of offsets in impeding asthenospheric flow, rather than the cooling effects on crustal magma chambers. In either case, we suggest that the overall differences in magma supply and offset distance are likely explanations for the lack of bathymetric depression and pronounced magmatic differentiation at 93°15′W. The presence of high Mg # at this offset suggests that erupted lavas did not experience prolonged residence in a shallow magma reservoir. Whether this is because the shallow AMC is disrupted at the OSC or rather that the dikes feeding the axis bypass a shallow AMC is unknown.

7. Plume-Ridge Interaction

[21] The GSC generally shoals in both directions toward the Galápagos Transform at ∼90.5°W (Figures 1 and 9). The thickest crust along the western GSC occurs between 91°W and 92°W [*Detrick et al.*, 2002; *Canales et al.*, 2002], coinciding with pronounced geochemical anomalies [*Schilling et al.*, 1982; *Verma and Schilling*, 1982; *Verma et al.*, 1983; *Cushman et al.*, 2001; *Schilling et al.*, 2003], indicating a strong influence from the nearby Galápagos hot spot. The point on

Table 2. Propagating Rifts

PR system	95.5°W	93.25°W
Spreading rate (mm/yr)[a]	48.7	52.2
Crustal thickness (km)[b]	5.7	6.4
Supply (x 10^6 m^3/km)	0.278	0.334
Propagation rate (mm/yr)[c]	34	70
Offset distance (km)	22.2	6.8
Bathymetric anomaly (m)[d]	∼250	−150
Fractionation anomaly length (km)	∼35	None

[a] From *DeMets et al.* [1994].
[b] From *Detrick et al.* [2002] using best-fit polynomial regression to seismic data.
[c] From *Wilson and Hey* [1995].
[d] Difference from regional bathymetric gradient. The 95.5° PR tip is 250 m deeper than the regional average, whereas the limbs of the 93.25° OSC are up to 150 m shallower than the regional average.

the western GSC closest to the center of the Galápagos hot spot, assumed to be Fernandina Island [e.g., *White et al.*, 1993], is near 91°10′W, about 25 km east of the shallowest portion of the spreading center (Figures 1 and 8a), and about 60 km east of the region showing the strongest hot spot geochemical signatures. This region also marks the intersection of the GSC with several volcanic chains that appear to emanate from just north of the main Galápagos archipelago to the south (Figure 9).

7.1. Wolf-Darwin and Associated Lineaments

[22] An intriguing feature of the Galápagos region is the presence of a series of volcanic chains that approach the GSC from the south between ∼92°30′W and 89°W (Figure 9). We have identified seven such lineaments, which appear to radiate away from the central part of the Galápagos Archipelago, a region where magmatic activity peaked more than 2 million years ago [*Geist et al.*, 1986; *White et al.*, 1993; *Harpp and Geist*, 2002]. The morphology of the chains suggests that they consist of multiple, locally coalesced volcanic centers.

[23] The origin of these lineaments has been a subject of considerable discussion [see *Harpp and Geist*, 2002]. Of the seven lineaments shown in Figure 9, the Wolf-Darwin Lineament (WDL) has received the most attention. *Morgan* [1978] proposed that the WDL is a second type of hot spot track that is a consequence of plume-ridge interaction. This hypothesis predicts that the volcanoes of the WDL formed at the point on the GSC closest to

Figure 9. (opposite) (a) Bathymetric map of the northern Galápagos platform and GSC, based on multibeam data of Figure 2 merged with satellite-derived seafloor topography data modified from *Smith and Sandwell* [1997]. (b) Same area as in Figure 9a, emphasizing the curved volcanic chains (yellow shading) radiating away from the northern Galápagos Archipelago. The plate boundary encompassing the GSC (light red shading) and Galápagos Transform is shown as a solid blue line. The Galápagos Fracture Zone (GFZ) extension of the Galápagos Transform is shown with dashed blue lines; the southern limit of the GFZ based on the study of *Wilson and Hey* [1995] (see text) is shaded. Numbers along the Wolf-Darwin Lineament (WDL) are ages in Ma from *White et al.* [1993] and *Sinton et al.* [1996]. GR is Genovesa Ridge. Crosses along each volcanic lineament are points used in linear regressions to determine average trend of each lineament. Solid blue lines are regressed lineament trends using all points. Solid red lines are regressed trends for black crosses only, i.e., excluding the two northernmost points (blue crosses) of each lineament. The azimuths and intersections of these trends on 1°N reference latitude (solid black line) are plotted in Figure 10. Circles lying just north of Santiago Island enclose the calculated centers of the radial patterns, determined from the relations in Figure 10; blue circle is the center of the blue trends and red circle is the center of the red trends. Because the volcanic lineaments tend to curve close to the ridge axis so that the intersection is at nearly right angles, we consider the red trends, i.e., those excluding the near-ridge curvature of the lineaments, to be a better estimate of the center of the radial pattern defined by the volcanic lineaments. Note the close correspondence of this circle to the southern limit of the age discontinuity across the GFZ. See text for discussion.

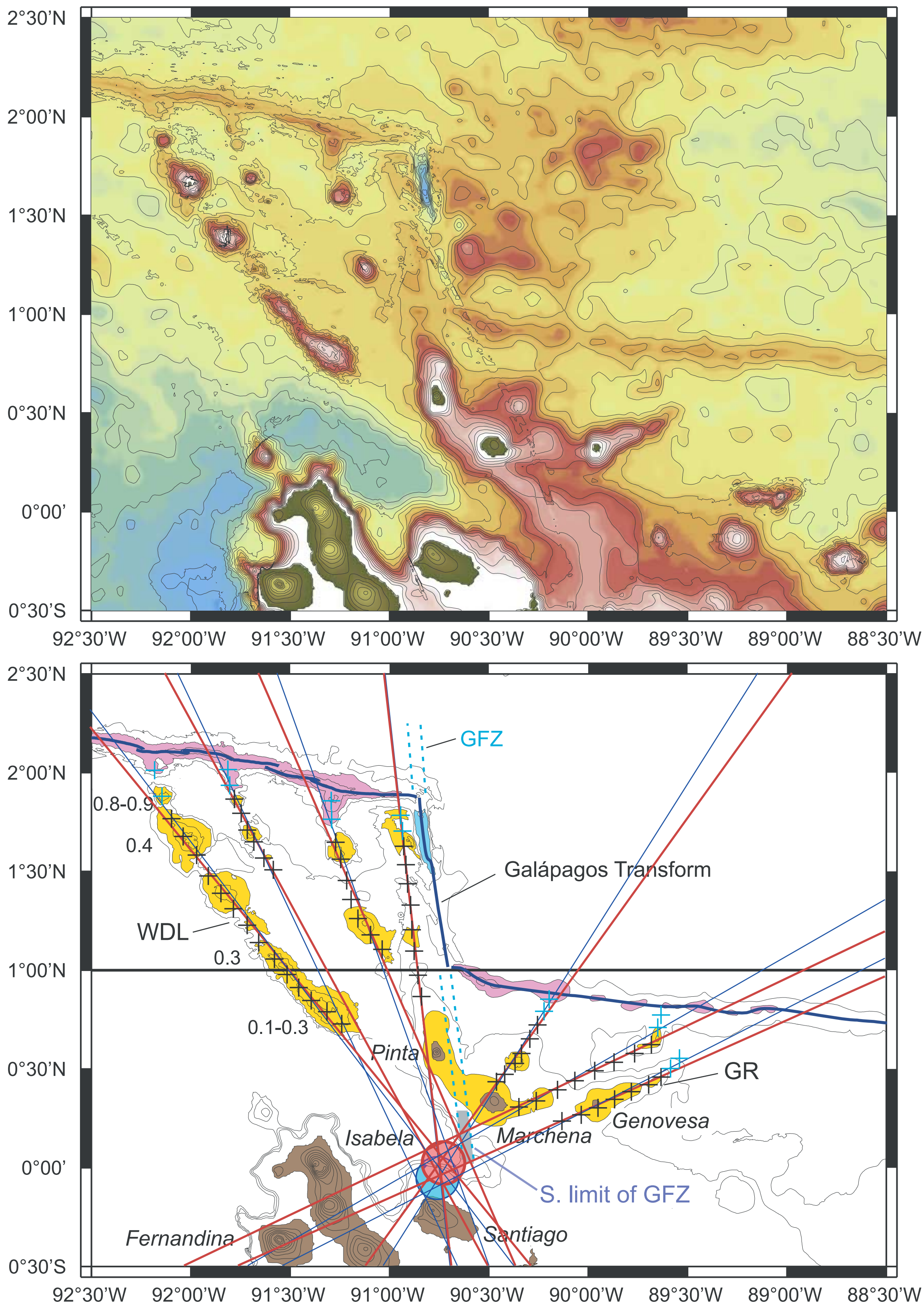
2°30'N
2°00'N
1°30'N
1°00'N
0°30'N
0°00'
0°30'S
92°30'W
92°00'W
91°30'W
91°00'W
90°30'W
90°00'W
89°30'W
89°00'W
88°30'W
GFZ
Galápagos Transform
0.8-0.9
0.4
WDL
0.3
0.1-0.3
Pinta
GR
Genovesa
Marchena
Isabela
S. limit of GFZ
Santiago
Fernandina

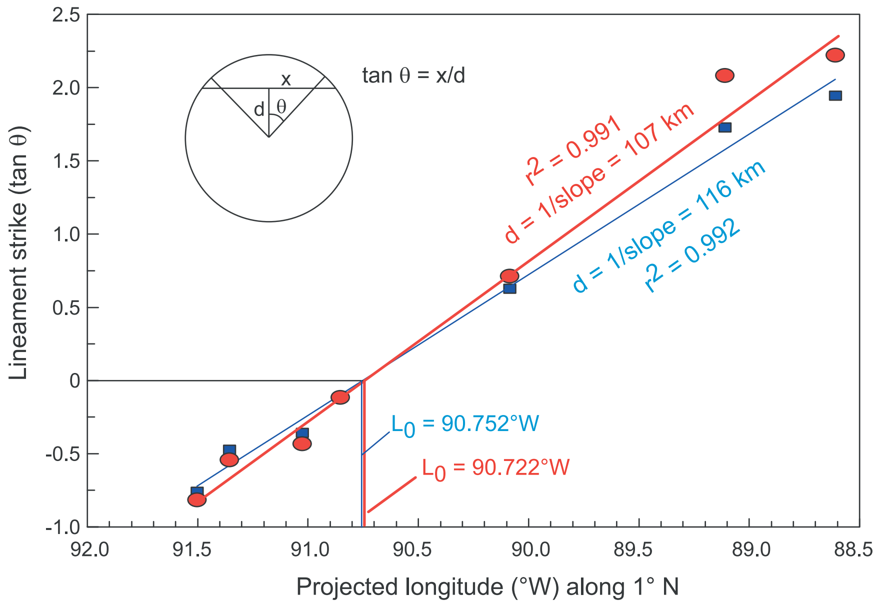

Figure 10. Plot showing the relationship between the orientation of the volcanic lineaments of Figure 9 and the longitude at which the lineament trends intersect 1°N reference latitude. Both the complete lineament trends (blue) and the lineaments excluding the northernmost, near-ridge points along the trends (red) show strong linearity, indicating that they can be described by a radial pattern (see inset) around an origin, or center of radiation. The origin of the complete lineament trends (blue) is 116 km south of 1°N along 90.752°W; the origin for lineaments, excluding the northernmost points (red), is 107 km south of 1°N along 90.722°W. These calculated centers are plotted on Figure 9.

the hot spot and subsequently migrated with plate motion. Some consequences of this hypothesis are that the ages of edifices along the WDL should correspond to the age of the lithosphere on which they formed, and that the geochemistry of lavas along the WDL should show an increasing contribution from plume sources to the south. *White et al.* [1993] and *Sinton et al.* [1996] showed that the ages of volcanoes along the WDL are much younger than, and possibly define a progression opposite to that, predicted by *Morgan* [1978] (Figure 9). Also, while *Verma et al.* [1983] argued that a local geochemical peak in plume influence near the WDL intersection supported *Morgan*'s [1978] hypothesis, *Harpp and Geist* [2002] noted that this would imply a location of the Galápagos hot spot more than 100 km west of Isla Fernandina. *Harpp and Geist* [2002] also demonstrated that the geochemical patterns are consistent with magma being derived from the local mantle beneath each volcanic edifice, rather than with lateral flow away from the hot spot. Thus the earlier models of *Morgan* [1978] and *Verma et al.* [1983] appear to be inconsistent with age, geometric and geochemical evidence from the WDL.

[24] An alternative possibility is that the WDL and other volcanic lineaments are controlled by the lithosphere. On the basis of gravity modeling, *Feighner and Richards* [1995] suggested that the WDL is a lithospheric fault. *Harpp and Geist* [2002] and *Harpp et al.* [2003] also favor a lithospheric control on the WDL and Genovesa Ridge, and specifically proposed that they formed as a consequence of oblique spreading associated with the Galápagos Transform, possibly analogous to extensional transform zones [*Taylor et al.*, 1994] along other oblique spreading centers.

[25] The overall geometry of the lineaments defines a radiating arcuate pattern. Those chains east of 90°30′W intersect the GSC east of the Galápagos Transform and are concave to the northwest, whereas the chains that intersect the western GSC are concave to the east (Figure 9). Close to the ridge axis the lineaments curve so that they

intersect the GSC at nearly right angles. The overall strike of the lineaments decreases in a regular pattern with distance from the central part of the region (Figures 9 and 10). Those close to the Galápagos transform zone strike nearly parallel to it (~357°), becoming more E-W with distance away from it. We have quantified the variation in lineament strike throughout the region by determining the average strike of the lineaments by regression of selected points along each trajectory (Figure 9). In order to eliminate possible near-ridge changes in strike of the lineaments, we also determined average strikes of the lineaments that exclude the two northernmost points in each trend (red lines in Figure 9b). A plot of lineament strike versus intersection longitude (Figure 10) shows that the distribution of measured azimuths can be described by a radial (spoke) pattern. The origin for the pattern defined by the complete lineaments lies along 90°45′W, 116 km south of 1°N. The trend for the lineaments, excluding the near-ridge northward bends indicates a center lying slightly farther to the northeast, along longitude 90°43′W, 107 km south of 1°N (Figures 9b and 10).

[26] The purpose of this simple analysis is to test quantitatively for the presence of a radial pattern that is already apparent by visual inspection of the bathymetry map. Although there are uncertainties in our method, we have produced an extremely coherent result, indicating a radial pattern emanating from a center just north of Santiago Island. Our analysis suggests that this center lies on the northern portion of the archipelago and near the same longitude as the Galápagos Transform. Although the oblique transform model of *Harpp and Geist* [2002] predicts opposite curvature to the observed pattern, the systematic relationship between lineament strike and distance from the fracture zone (Figure 9) argues for a role of the Galápagos Fracture Zone in the development of zones of lithosopheric weakness in this region.

[27] According to *Wilson and Hey* [1995], the present Galápagos Transform formed between 3.6 and 2.6 Ma. Spreading rates at that longitude were ~56.5 mm/yr prior to 1.5 Ma, and ~60.9 mm/yr since 1.5 Ma [*Wilson and Hey*, 1995, Figure 4]. Therefore assuming symmetric accretion, the limit of the age discontinuity in the lithosphere marked by the fracture zone lies about 77–105 km south of the present intersection of the Galápagos Transform with the eastern GSC, very close to our inferred center of the radial pattern, especially when the near-ridge curvature is excluded from the regression analysis. Uncertainties in defining the fracture zone limit arise from the assumption of symmetrical accretion as well as the spreading rate determinations by *Wilson and Hey* [1995]. Despite the lack of precision in this analysis, it is clear that arcuate volcanic lineaments have formed in lithosphere with an age discontinuity across the ~90°40′W fracture zone, but not farther south where such an age discontinuity does not exist (Figure 9b). Within the uncertainties, it is possible that these lineaments radiate from a point where the age discontinuity associated with the ~90°40′W fracture zone first appears. This would allow for the possibility of the fracture zone influencing volcanic lineament formation, geometry, or both.

[28] Independent of the possible fracture zone effect, a likely explanation for the origin of the volcanic lineaments is that they are following stress trajectories in the lithosphere, possibly as a result of the plume impinging on the base of the lithosphere. Lithospheric uplift of an axisymmetric plume is predicted to generate circumferential tension with the least tensile directions radiating in a spoke pattern [*White and McKenzie*, 1995; *Ernst and Buchan*, 1997]. Magma generated below the lithosphere will exploit this stress pattern, tending to open dikes and form lineaments parallel to the least tensile direction. What is perplexing is that the apparent center of the radial pattern in the Galápagos area is displaced more than 90 km NE of the present location of the Galápagos plume center inferred from age and geochemical data [*White et al.*, 1993], and lies close to a deep trough between Santiago and Pinta islands. In addition, the lineaments curve so that they intersect the GSC at nearly right angles; if indeed the lineaments follow trajectories of least tension far from the spreading center, this explanation is unlikely to be the case at the GSC where least tension is parallel to the ridge axis.

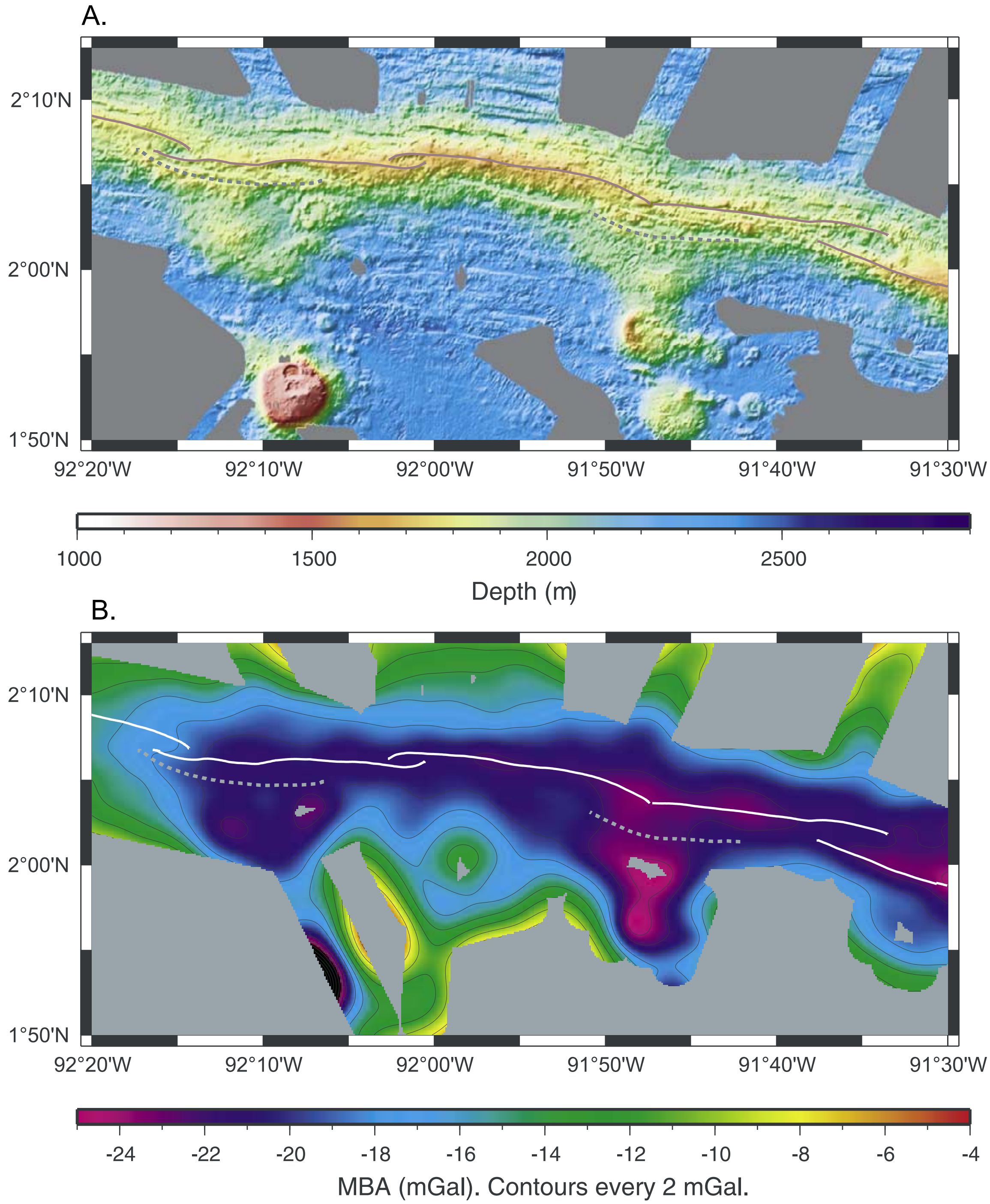

Figure 11. Maps of the area where two volcanic lineaments intersect the GSC. (a) Bathymetry. The current axis is shown as a solid line; abandoned rifts as dashed lines. (b) Mantle Bouguer Anomaly (MBA), calculated by subtracting the effects of the seafloor-water ($\Delta\rho$ = 1800 kg/m^3) and crust-mantle ($\Delta\rho$ = 500 kg/m^3) interfaces from free-air gravity, assuming a crustal layer of constant thickness (6 km). Current axis and abandoned rifts are shown by solid and dashed lines, respectively. Note that MBA lows coincide with bathymetric lows at the intersections; see text for discussion.

[29] In the Galápagos area, the stress regime is almost certainly complicated by regional stresses, including those associated with the Galápagos Transform, age discontinuities across the Galápagos Fracture Zone, distortion of the plume as it is deflected by velocity shear in the upper asthenosphere [*White et al.*, 1993], possible discontinuities in lithospheric strength [*Feighner and Richards*, 1995], as well as by large gradients in lithospheric thickness due to cooling. Although we do not fully understand the ultimate cause of the lineaments present in this area, we are in general agreement with *Harpp and Geist* [2002] that these zones of weakness can be locally in tension, and exploited as pathways for volcanic activity during times of increased magma flux.

7.2. Effects on Spreading Center Processes

[30] Although the overall strike of the GSC in the Eastern Province is relatively constant at ~280°, the axis steps to the south where the lineaments intersect the spreading center. This southward displacement is accommodated by OSCs that step left east of the intersections and step to the right west of the intersections. South of the present axis within the intersection areas are arcuate ridges that we interpret to be abandoned OSC limbs (Figures 11 and 12).

[31] The intersection areas are generally characterized by bathymetric and mantle Bouguer gravity anomaly (MBA) lows relative to the GSC on either side (Figure 11); the MBA low is most pronounced at the eastern intersection near 91°47′W. The deeper bathymetry can partly be attributed to the presence of OSC limbs in the intersection areas, suggesting that magma supply is partitioned between opposing spreading center limbs [*Sempere and Macdonald*, 1986]. The wavelength of the negative MBA anomalies is ~15 km, indicating the presence of low-density material confined to the crust or uppermost mantle; deeper low-density material would produce anomalies with greater wavelengths. The coincidence of bathymetric lows with MBA lows is unexpected because, if the crust is in isostatic equilibrium, topographically low regions are expected to have relatively thin crust and thus produce MBA highs. These observations therefore suggest the presence of relatively shallow, low-density material, but with lithospheric stresses large enough to overcome the buoyancy of this material and depress the seafloor.

[32] A possible source of this anomalous material is unusually low-density crust, possibly a result of extensive fracturing during repeated spreading center reorganizations (see below). This interpretation is supported by the recognition of low-seismic-velocity crust at the 9°03′N OSC on the East Pacific Rise [*Bazin et al.*, 2003; *Canales et al.*, 2003]. Another possibility is that the crust is slightly thicker. Indeed, thickened crust beneath the off-axis portion of the associated volcanic lineaments is consistent with bathymetric highs corresponding with MBA lows there.

[33] Some combination of the above possibilities can explain the MBA lows, but would not, in isolation, explain why the ridge axis is deeper in these regions. The coincidence of MBA lows with deep bathymetry could arise from interactions between the volcanic lineaments and the spreading center. For example, if the lineaments behave as giant magma-filled cracks, then the region near the tips of these cracks are expected to be regions with locally high tension [e.g., *Pollard and Aydin*, 1984]. Excess faulting in these zones may reduce crustal density by introducing porosity, but in addition, it may be possible that the combination of anelastic strain and associated moments generated in the lithosphere at the intersections may dynamically depress topography, possibly in a manner similar to that which may be responsible for the formation of axial valleys at slow spreading ridges [*Chen and Morgan*, 1990]. Quantitative models are needed to test whether this mechanism can sufficiently depress the seafloor, but the prediction of enhanced tensile stress near the tips of these volcanic lineaments predicts dynamic effects at least in the right sense (i.e., downward).

[34] Our interpretation of the evolution of the intersection areas is shown in Figure 12. A basic tenet of this interpretation is that the spreading center is active more or less continuously, whereas the lineaments are active only intermittently. Volcanism

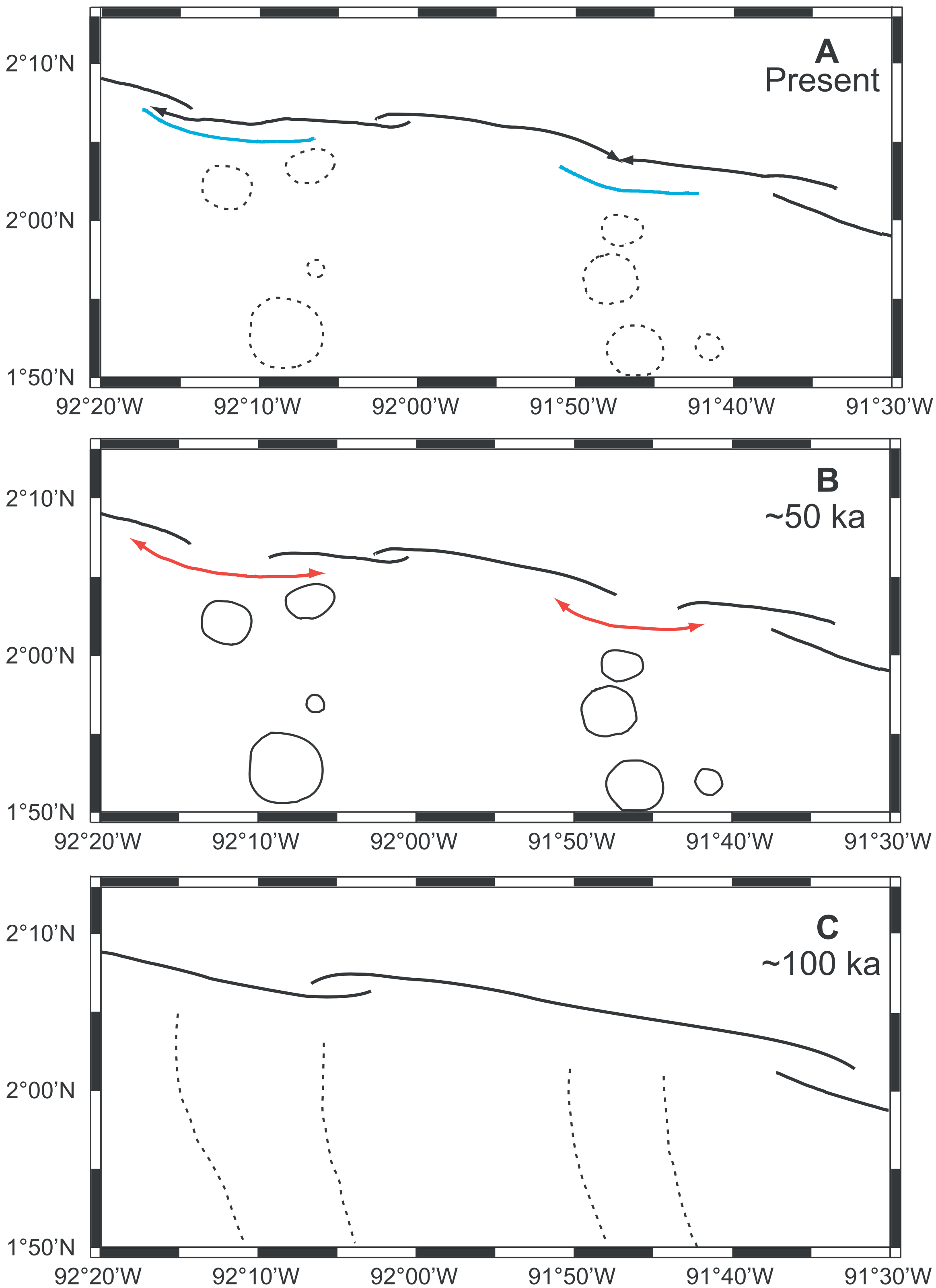
A
Present
2°10'N
2°00'N
1°50'N
92°20'W
92°10'W
92°00'W
91°50'W
91°40'W
91°30'W
B
~50 ka
C
~100 ka

along the extensional lineaments is presumably enhanced during periods of overall increased supply in the plume region. At such times magma can rise along zones of weakness, as proposed by *Harpp and Geist* [2002]. During such times, lithospheric weakening between the spreading center and the plume favors reorganization of the spreading center with southward jumps in the axis. When the period of lineament volcanism ceases, the spreading center attempts to straighten by rift propagation, which results in the abandonment of decapitated OSC limbs, similar to processes described by *Macdonald et al.* [1987] for fast spreading ridges. The spacing between the abandoned limbs and the present axis is on the order of 2–3 km. Assuming symmetrical spreading at current rates (54 mm/yr at 92°W according to Nuvel 1A [*DeMets et al.*, 1994]), the short-lived propagation and decapitation events have occurred within the last 40–55 ka. This time is later than the youngest dated activity within the volcanic lineaments (Figure 9), supporting the tectonic interpretation outlined here.

[35] There are many uncertainties in this scenario of short-lived spreading center reorganizations. Evidence from the WDL suggests that it has been intermittently active in the last 1 Myr, but it is presently unknown if all of the lineaments have been active simultaneously, or how many periods of activity might be responsible for the volcanic edifices along any one of them. If volcanic activity along the lineaments is triggered by pulsing of the Galápagos plume, then it is likely that many pre-existing weaknesses in the plate might be simultaneously activated. Although we show most of the near-ridge volcanoes in the region of Figure 11 as having formed in the most recent pulse, they could equally be a consequence of several short-lived events in the last 850 ka, the approximate age of the lithosphere beneath the volcanoes near 1°50′N. However, despite these uncertainties, the general scenario of short-lived, southward steps in the GSC axis, followed by rift propagation and local rift abandonment results in a significant number of right-stepping offsets along the GSC, a feature that is primarily restricted to the Eastern Province of the GSC where ridge-hot spot interaction is maximized west of the Galápagos Transform.

[36] The scenario outlined above and in Figure 12 is generally similar to that of *Wilson and Hey* [1995] for episodic southward jumps in the axis close to the hot spot, but at much shorter temporal and spatial scales. The two scales of segmentation may be closely linked, however. It is likely that the major southward jumps in the axis that ultimately led to major propagating rift systems and the primary segmentation of the GSC also were localized in the zones where the radiating volcanic lineaments intersect the GSC. We suppose that these large-scale reorganizations began with relatively small-scale jumps occurring more or less simultaneously at several closely spaced intersections. These small offsets can then join to produce a stable rift segment that can evolve into a major propagating rift. In other cases, however, small southward steps in rifting may be too intermittent or too widely spaced such that a major shift in the ridge segment does not occur. This appears to be the case with the isolated rift offsets that have occurred recently at the intersections of the WDL and the lineament near 92°47′W, which apparently became unstable and abandoned by subsequent propagation events on pre-existing segments.

8. Conclusions

[37] New multibeam mapping of the GSC between 90°40′W and 98°W has allowed us to define the fine-scale morphology and segmentation of the

Figure 12. (opposite) Interpretative diagrams showing the evolution of ridge segments at the intersection area of volcanic lineaments shown in Figure 11. Lower panel (∼100 ka) shows hypothetical simple ridge structure; dashed lines outline lithospheric zones of weakness, not necessarily active at that time. Middle panel (∼50 ka) shows time of increased volcanic activity at the plume, when lineaments become activated with the eruption of volcanoes (circled areas). At this time, weakened lithosphere to the south favors development of new segments of the ridge axis, stepping to the south along a series of small OSCs. Top panel (present) results when lineaments are no longer active; southernmost OSC limbs are abandoned by propagation of longer or shallower segments as the ridge attempts to straighten. Note that additional right-stepping offsets are produced during this evolutionary scheme.

spreading center. At the coarsest scale the region can be separated on the basis of major propagating rift offsets into three provinces with differing average strike of the axis, axial morphology, axial depth and roughness. Farthest from the Galápagos hot spot, the Western Province, west of 95°30′W, strikes nearly east-west and is characterized by a series of segments with axial deep morphology that are separated by non-transform offsets. The ridge strike becomes increasingly NW to the east, averaging ∼276° in the Middle Province, and ∼280° in the Eastern Province. The Middle Province, between the PR tips at 93°15′W and 95°30′W has transitional axial morphology. Between the Galápagos Transform near 90°40′W and 93°15′W the GSC axis in the Eastern Province is mainly less than 1800 m deep and characterized by an axial high morphology. At a finer scale, the axial region can be divided into 32 smaller segments on the basis of offsets mainly less than 2 km. In the Western and Middle Provinces these offsets are mainly left-stepping, but in the Eastern Province, right-stepping offsets formed as a consequence of ridge re-orientation during times of high productivity associated with the Galápagos plume. Variations in glass Mg # indicate that the GSC is segmented magmatically into 8 broad regions. The boundaries between these regions mainly correspond with the larger physical offsets in the axis, or significant changes in the character of the axial magma chamber. Within the Middle Province, glass Mg # tends to be less variable locally where axial magma chambers are smaller or more ephemeral than detected by MCS reflection imaging, compared to regions where there is a well-defined AMC.

[38] The propagating rifts at 93°15′W and 95°30′W show striking differences in axial depth and extent of lava fractionation. Close to the 95°30′W PR tip, the axis is anomalously deep and lavas from this region are highly fractionated. In contrast, the overlapping limbs of the PR at 93°15′W are unusually shallow and lavas from this zone have the highest Mg # of any in the Eastern and Middle Provinces. These differences probably reflect the ∼17% lower overall magma supply and ∼3x greater offset distance at the 95°30′W tip. The new regional mapping suggests that the doomed North Graben rift at 95°30′W is probably the last vestige of a pre-existing axial deep segment, rather than a migrating extensional relay zone, as proposed by *Kleinrock et al.* [1989].

[39] The structure of the Eastern Province, which is the region closest to the Galápagos Archipelago, is complicated by the intersection of a series of volcanic lineaments that appear to radiate away from a point located on the northern edge of the Galápagos platform. As these lineaments approach the GSC from the south they bend so that their intersection angles are nearly orthogonal to the ridge axis. At the intersection areas, the GSC axis is displaced to the south, a displacement that is accommodated by south-stepping OSCs. We have identified arcuate ridges in the bathymetry that lie farther south than the present axis in the intersection areas, which we interpret to be abandoned OSC limbs from earlier southward displacements of the axis. We propose that southward displacement of the axis at the intersection areas is promoted during intermittent times of increased plume activity, when lithospheric zones of weakness can become volcanically active. Following cessation of the increased plume activity, the axis attempts to straighten by decapitating southernmost OSC limbs during short-lived propagation events. This process results in an unusual number of right stepping offsets in the Eastern Province, relative to the rest of the GSC.

Acknowledgments

[40] We are grateful to the Captain, crew and shipboard scientific party of R/V *Maurice Ewing* Cruise EW0004 for their help with data acquisition at sea. The Ecuadorian government and the Parque Nacional Galápagos permitted work in their territorial waters. We are grateful to Dan Fornari for access to multibeam data from the AHA-NEMO2 cruise, and to Reinhard Werner and Kaj Hoernle for multibeam data from R/V *Sonne* Cruise 158. Discussions with Buffy Cushman, Richard Hey, and Jian Lin were helpful in various aspects of this study. The MB-System software package of David Caress and Dale Chayes was used extensively in the processing of multibeam bathymetric data. Many figures in this paper were prepared using the GMT software package [*Wessel and Smith*, 1998]. We greatly appreciate careful and detailed reviews by Denny Geist, Associate Editor David Graham and an anonymous reviewer on an earlier version of this paper. This work was supported by NSF grants OCE98-18632 to the University of Hawai'i and OCE98-19117 to the Woods Hole Oceanographic Institution; support was provided

to M. B. by a CIW/DTM Postdoctoral Fellowship. This is SOEST contribution number 6291 and WHOI contribution number 11038.

References

Barckhausen, U., C. R. Ranero, R. Von Huene, S. C. Cande, and H. A. Roeser, Revised tectonic boundaries in the Cocos Plate off Costa Rica: Implications for the segmentation of the convergent margin and for plate tectonic models, *J. Geophys. Res.*, *106*, 19,207–19,220, 2001.

Bazin, S., et al., A three-dimensional study of a crustal low velocity region beneath the 9°03′N overlapping spreading center, *Geophys. Res. Lett.*, *30*(2), 1039, doi:10.1029/2002GL01537, 2003.

Behn, M. D., J. M. Sinton, and R. S. Detrick, Effect of the Galápagos hotspot on seafloor volcanism along the Galápagos Spreading Center (90.9°–97.6°W), *Earth Planet. Sci. Lett.*, in press, 2003.

Blacic, T., G. Ito, R. Detrick, J. P. Canales, and J. Sinton, Shallow crustal structure along the western Galápagos Spreading Center 91.3° to 95.2°W: Correlations between axial magma lens, layer 2A and axial topographic characteristics, *Eos Trans. AGU*, *83*(47), Fall Meeting Suppl., Abstact T72C-01, 2002.

Canales, J. P., J. J. Dañobeitia, R. S. Detrick, E. E. E. Hooft, R. Bartolome, and D. F. Naar, Variations in axial morphology along the Galápagos Spreading Center and the influence of the Galápagos hotspot, *J. Geophys. Res.*, *102*, 27,341–27,354, 1997.

Canales, J. P., G. Ito, R. S. Detrick, and J. Sinton, Crustal thickness along the western Galápagos spreading center and the compensation of the Galápagos hotspot swell, *Earth Planet. Sci. Lett.*, *203*, 311–327, 2002.

Canales, J. P., R. S. Detrick, D. R. Toomey, and W. D. S. Wilcock, Segment-scale variations in the crustal structure of 150–300 kyr old fast spreading oceanic crust (East Pacific Rise, 8°15′N–10°5′N) from wide-angle seismic refraction profiles, *Geophys. J. Int.*, *152*, 766–794, 2003.

Carbotte, S. M., and K. C. Macdonald, The axial topographic high at intermediate and fast spreading ridges, *Earth. Planet. Sci. Lett.*, *128*, 85–97, 1994.

Chen, Y., and W. J. Morgan, Rift valley/no rift valley transition at mid-ocean ridges, *J. Geophys. Res.*, *95*, 17,571–17,581, 1990.

Christie, D. M., and J. M. Sinton, Evolution of abyssal lavas along propagating segments of the Galapagos Spreading Center, *Earth Planet. Sci Lett.*, *56*, 321–335, 1981.

Cushman, B. J., J. E. Dixon, D. Graham, and J. M. Sinton, Plume-affected geochemical trends in along-axis samples from the Galápagos Spreading Center, 90°30′W to 98°W, *Eos Trans. AGU*, *82*(47), Fall Meet. Suppl., Abstract T42B-0930, 2001.

DeMets, C., R. G. Gordon, D. F. Argus, and S. Stein, Effect of recent revisions to the geomagnetic reversal time scale on estimates of current plate motions, *Geophys. Res. Lett.*, *21*, 2191–2194, 1994.

Detrick, R. S., J. M. Sinton, G. Ito, J. P. Canales, M. Behn, T. Blacic, B. Cushman, J. E. Dixon, D. W. Graham, and J. J. Mahoney, Correlated geophysical, geochemical, and volcanological manifestations of plume-ridge interaction along the Galápagos Spreading Center, *Geochem. Geophys. Geosyst.*, *3*(10), 8501, doi:10.1029/2002GC000350, 2002.

Ernst, R. E., and K. L. Buchan, Giant radiating dyke swarms: Their use in identifying pre-Mesozoic large igneous provinces and mantle plumes, in *Large Igneous Provinces: Continental, Oceanic, and Planetary Flood Volcanism*, *Geophys. Monogr. Ser.*, vol. 100, edited by J. J. Mahoney and M. F. Coffin, pp. 297–333, AGU, Washington, D. C., 1997.

Feighner, M. A., and M. A. Richards, Lithospheric structure and compensation mechanisms of the Galápagos Archipelago, *J. Geophys. Res.*, *99*, 6711–6729, 1995.

Geist, D. J., A. R. McBirney, and R. A. Duncan, Geology and petrology of lavas from San Cristobal Island, Galápagos Archipelago, *Geol. Soc. Am. Bull.*, *97*, 555–556, 1986.

Harpp, K., and D. Geist, Wolf-Darwin lineament and plume-ridge interaction in northern Galápagos, *Geochem. Geophys. Geosyst.*, *3*(11), 8504, doi:10.1029/2003GC000370, 2002.

Harpp, K. S., D. J. Fornari, D. J. Geist, and M. D. Kurz, Genovesa Submarine Ridge: A manifestation of plume-ridge interaction in the northern Galápagos Islands, *Geochem. Geophys. Geosyst.*, *4*(9), 8511, doi:10.1029/2002GC000531, 2003.

Hey, R. N., Tectonic evolution of the Cocos-Nazca spreading center, *Geol. Soc. Am. Bull.*, *88*, 1404–1420, 1977.

Hey, R. N., M. Kleinrock, S. P. Miller, T. M. Atwater, and R. C. Searle, Sea Beam/Deep-Tow investigations of an active oceanic propagating rift system, Galápagos 95.5°W, *J. Geophys. Res.*, *91*, 3369–3393, 1986.

Hey, R. N., J. M. Sinton, and F. K. Duennebier, Propagating rifts and spreading centers, in *The Geology of North America, Vol. N: The Eastern Pacific Ocean and Hawaii*, edited by E. L. Winterer, pp. 161–176, Geol. Soc. of Am., Boulder, Colo., 1989.

Hey, R. N., et al., ALVIN investigation of an active propagating rift system, Galapagos 95.5°W, *Mar. Geophys. Res.*, *14*, 207–226, 1992.

Kleinrock, M. C., and R. N. Hey, Detailed tectonics near the tip of the Galapagos 95.5°W propagator: How the lithosphere tears and a spreading center axis develops, *J. Geophys. Res.*, *94*, 13,801–13,838, 1989.

Kleinrock, M. C., R. C. Searle, and R. N. Hey, Tectonics of the failing spreading center system associated with the 95.5°W Galapagos propagator, *J. Geophys. Res.*, *94*, 13,839–13,857, 1989.

Langmuir, C. H., J. F. Bender, and R. Batiza, Petrological and tectonic segmentation of the East Pacific Rise, 5°30′–14°30′N, *Nature*, *322*, 422–429, 1986.

Lonsdale, P., Nontransform offsets of the Pacific-Cocos plate boundary and their traces on the rise flank, *Geol. Soc. Am. Bull.*, *96*, 313–327, 1985.

Macdonald, K. C., Mid-ocean ridges: Fine scale tectonic, volcanic and hydrothermal processes within the plate boundary zone, *Ann. Rev. Earth Planet. Sci.*, *10*, 155–190, 1982.

Macdonald, K. C., and P. J. Fox, The axial summit graben and cross-sectional shape of the East Pacific Rise as indicators of axial magma chambers and recent volcanic eruptions, *Earth Planet. Sci. Lett.*, *88*, 119–131, 1988.

Macdonald, K. C., J.-C. Sempere, P. J. Fox, and R. Tyce, Tectonic evolution of ridge-axis discontinuities by the meeting, linking, or self-decapitation of neighboring ridge segments, *Geology*, *15*, 993–997, 1987.

Meschede, M., and U. Barckhausen, Plate tectonic evolution of the Cocos-Nazca spreading center, *Proc. Ocean Drill. Program, Sci. Results*, *170*, 1–10, 2001.

Morgan, W. J., Rodriguez, Darwin, Amsterdam, . . ., A second type of hotspot island, *J. Geophys. Res.*, *83*, 5355–5360, 1978.

Nelson, K. D., A simple thermal-mechanical model for mid-ocean ridge topographic variations, *R. Astron. Soc. Geophys. J.*, *65*, 19–30, 1981.

Phipps Morgan, J., and E. M. Parmentier, Causes and rate-limiting mechanisms of ridge propagation: A fracture mechanics model, *J. Geophys. Res.*, *90*, 8603–8612, 1985.

Pollard, D. P., and A. Aydin, Propagation and linkage of oceanic ridge segments, *J. Geophys. Res.*, *89*, 10,017–10,028, 1984.

Scheirer, D. S., and K. C. Macdonald, Variation in cross-sectional area of the axial ridge along the East Pacific Rise: Evidence for the magmatic budget of a fast-spreading center, *J. Geophys. Res.*, *98*, 7871–7885, 1993.

Schilling, J.-G., R. N. Anderson, and P. Vogt, Rare earth, Fe and Ti variations along the Galapagos Spreading Centre and their relationship to the Galapagos mantle plume, *Nature*, *261*, 108–113, 1976.

Schilling, J.-G., R. H. Kingsley, and J. D. Devine, Galápagos hot spot-spreading center system: 1. Spatial petrological and geochemical variations (83°W–101°W), *J. Geophys. Res.*, *87*, 5593–5610, 1982.

Schilling, J.-G., D. Fontignie, J. Blichert-Toft, R. Kingsley, and U. Tomza, Pb-Hf-Nd-Sr isotope variations along the Galápagos Spreading Center (101°–83°W): Constraints on the dispersal of the Galápagos mantle plume, *Geochem. Geophys. Geosyst.*, *4*(10), 8512, doi:10.1029/2002GC000495, 2003.

Searle, R. C., Location and segmentation of the Cocos-Nazca Spreading Centre West of 95°W, *Mar. Geophys. Res.*, *11*, 15–26, 1989.

Sempere, J.-C., and K. C. Macdonald, Overlapping spreading centers: Implications from crack growth simulation by the displacement discontinuity method, *Tectonophys.*, *5*, 151–163, 1986.

Sinton, C. W., D. M. Christie, and R. A. Duncan, Geochronology of Galápagos Seamounts, *J. Geophys. Res.*, *101*, 13,689–13,700, 1996.

Sinton, C. W., R. A. Duncan, M. Storey, J. Lewis, and J. J. Estrada, An oceanic flood basalt province within the Caribbean plate, *Earth Planet. Sci. Lett.*, *155*, 221–235, 1998.

Sinton, J. M., and R. S. Detrick, Mid-ocean ridge magma chambers, *J. Geophys. Res.*, *97*, 197–216, 1992.

Sinton, J. M., D. S. Wilson, D. M. Christie, R. N. Hey, and J. R. Delaney, Petrological consequences of rift propagation on oceanic spreading ridges, *Earth Planet. Sci. Lett.*, *62*, 193–207, 1983.

Sinton, J. M., S. M. Smaglik, J. J. Mahoney, and K. C. Macdonald, Magmatic processes at superfast spreading mid-ocean ridges: Glass compositional variations along the East Pacific Rise, 13°–23°S, *J. Geophys. Res.*, *96*, 6133–6155, 1991.

Sinton, J., R. Detrick, G. Ito, J. P. Canales, B. Cushman, M. Behn, T. Blacic, J. E. Dixon, D. Graham, J. Lin, J. Mahoney, and the Shipboard Scientific Party, Seismic and Petrologic Investigation of the Effects of Plume-Ridge Interaction at the Galápagos Spreading Center, *InterRidge News*, *9*(2), 41–45, 2000.

Smith, W. H. F., and D. T. Sandwell, Global seafloor topography from satellite altimetry and ship depth soundings, *Science*, *277*, 1957–1962, 1997.

Taylor, B., K. Crook, and J. Sinton, Extensional transform zones and oblique spreading centers, *J. Geophys. Res.*, *99*, 19,707–19,718, 1994.

Verma, S. P., and J.-G. Schilling, Galápagos hot spot-spreading center system: 2. ^{87}Sr/^{86}Sr and large ion lithophile element variations (85°W–101°W), *J. Geophys. Res.*, *87*, 10,838–10,856, 1982.

Verma, S. P., J.-G. Schilling, and D. G. Waggoner, Neodymium isotopic evidence for Galápagos hotspot-spreading centre system evolution, *Nature*, *306*, 654–657, 1983.

Vogt, P. R., Plumes, subaxial pipe flow and topography along the mid-ocean ridge, *Earth Planet. Sci. Lett.*, *29*, 309–325, 1976.

Wessel, P., and W. H. F. Smith, New, improved version of the Generic Mapping Tools released, *EOS Trans. AGU*, *79*, 579, 1998.

White, R. S., and D. McKenzie, Mantle plumes and flood basalts, *J. Geophys. Res.*, *100*, 17,543–17,585, 1995.

White, W. M., A. R. McBirney, and R. A. Duncan, Petrology and geochemistry of the Galápagos Islands: Portrait of a pathological mantle plume, *J. Geophys. Res.*, *98*, 19,533–19,563, 1993.

Wilson, D. S., and R. N. Hey, History of rift propagation and magnetization intensity for the Cocos-Nazca spreading center, *J. Geophys. Res.*, *100*, 10,041–10,056, 1995.